Exploring new insights in BAlN from evolutionary algorithms ab initio computations

H. Maiz Hadj Ahmed, H. Benaissa, Ali Zaoui, M. Ferhat

Exploring new insights in BAlN from evolutionary algorithms *ab initio* computations

H. Maiz Hadj Ahmed[1], H. Benaissa[1], A. Zaoui[2,*] and M. Ferhat[1]

[1]*Département de Génie Physique, (LPMF). Université des Sciences et de la Technologie d'Oran, Mohamed Boudiaf. Oran, Algeria.*
[2]*LGCgE, Polytech'Lille. Université de Lille 1 Sciences et Technologies.*

Avenue Paul Langevin. 59655 Villeneuve D'Ascq Cedex, France.

ABSTRACT

BN-AlN alloys are potential candidates to achieve wide band gap material for ultraviolet device applications. By combing density functional theory and evolutionary structure predictions, we systematically explore the thermodynamic, mechanical, dynamical and optical properties of $B_xAl_{1-x}N$ alloys. Through structure search, three compounds (cubic (BAl_3N_4, and B_3AlN_4, space group *P*-43m), and tetragonal ($BAlN_2$, space group *P*-42m)) have been predicted. The calculated relative large formation enthalpies suggest that large miscibility gap exists in BAlN alloys. In addition, computed elastic constants and phonon show that these structures are mechanically and dynamically stable. From the state of the art LDA-1/2 we show that the direct band gap of BN-AlN evinces strong deviation from a linear dependence on B composition. We found -in particular- giant direct band gap bowing parameter of b~11.6eV for the entire range of composition, where b parameter is found to be sensitive to composition x. From a detailed analysis of the physical origin of the optical gap bowing b, we found that structural and chemical contributions play the most significant effects behind the huge optical band gap bowing parameter of BAlN alloys.

Keywords: *$B_xAl_{1-x}N$ alloys; evolutionary algorithm; density functional theory (DFT); mechanical, dynamical and optical properties; optical band gap bowing parameter.*

*Corresponding author: azaoui@polytech-lille.fr

1 Introduction

InGaN and AlGaN ternary III-V alloys based on wurtzite AlN, GaN and InN have recently revolutionized lighting industry and paved the way for efficient visible and ultra-violet light emitting diodes (LEDs). This was awarded the 2014 Nobel price of Physics.

Compared to the well-studied III-V-N (AlGaN, InGaN, AlInN) alloys, the research involving common-anion nitride based ternary alloys such as $B_xAl_{1-x}N$ is still at its early stage. Recently wurtzite BAlN alloys have been the subject of several experimental [1-4] and theoretical [5-6] studies.

A fundamental property while designing optoelectronic devices of semiconductors alloys is the variation of the fundamental direct energy gap $E_g(x)$ with composition x, which is a prerequisite for band gap engineering in order to fulfill devices applications. Unfortunately the variation of $E_g(x)$ differs from the simplest Vegard's linear 'law', but has a quadratic form, i.e., it exhibits bowing parameter b. Traditionally to model such alloys, two methods are currently used: (i) virtual crystal approximation (VCA), and (ii) supercells methods. Methods such as VCA are disqualified for any serious study of semiconductors alloys [7]; whereas by means of methods such as (ii) accurate results can -in principle- be obtained with large supercells. Nevertheless, such an approach requires very large supercells [8-13] to adequately reproduce the statistics of random alloys.

In the present study, we opted for a novel strategy to describe accurately the band gap dependence on B composition of $B_xGa_{1-x}N$ alloys. We use an evolutionary algorithm within the density functional theory (DFT) to find all possible stable phases in the BAlN alloys at ambient conditions. We also analyse the band gaps and the optical band gap bowing parameter of BAlN alloys. In addition, the mechanical and dynamical properties of BAlN alloys will be also discussed.

2 Computational details

Using the evolutionary algorithm approach as implemented in Material project database [14-15] we explore all possible state phases of BAlN alloys. In the framework of density functional theory (DFT) [16] using a plane-wave basis set. The underlying total-energy calculations were carried out by the Quantum ESPRESSO Package code [17]. The exchange-correlation term was approximated by the linearized density approximation (LDA) [18]. The interaction between the ions and the electrons are described by the projector-augmented wave pseudopotential scheme (PAW) [19]. We used a plane-wave energy cut-off of 65 Ry, and an energy cut-off of 600 Ry was included for the charge density. The Brillouin zone integrations was sampled at a higher level of accuracy using a finer Monkhorst-Pack [MP] [20] mesh of 10×10×8 for $BAlN_2$ and 12×12×12 for BAl_3N_4 and B_3AlN_4. The phonon properties are calculated using the density functional perturbation theory (DFTP) [21]. A 4 × 4 × 3, 2 × 2 × 2, and 2 × 2 × 2 *q*-points MP mesh has been used to perform inverse Fourier transformation for $BAlN_2$, BAl_3N_4, and B_3AlN_4 respectively. The atomic positions, lattice parameters and cell volume were fully relaxed until the forces on each atom were less than $1meVÅ^{-1}$. The total energy was converged to within 1meV/cell.

3 Results and Discussion

The analysis of the evolutionary algorithm gives a list of three candidate phases of $B_xAl_{1-x}N$ alloys: BAl_3N_4 (x = 0.25, cubic phase, space group P-43m), $BAlN_2$ (x = 0.5, tetragonal phase, space group P-4m2), and B_3AlN_4 (x = 0.75, cubic phase, space group P-43m). For all the predicted structures shown in Figure 1, the corresponding structural information is listed in Table I.

The calculated lattice constant a, and c/a ratio of wurtzite (WZ) BN and AlN are in good agreement with experimental measurements. Figure 2 displays the variation of the lattice parameter a and the lattice constant ratio c/a versus the composition x. Small deviations from Vegard-like law is found. The calculated bowing for a and c/a are ~0.11Å and ~0.60 respectively.

Thermodynamic stability of BAlN alloys is quantified by determining the alloy mixing enthalpy defined as:

$$\Delta H = E(x) - (1-x)\, E(\mathrm{AlN}) - x\, E(\mathrm{BN})$$

Where $E(x)$ is the total energy of the alloy at composition x, and E(AlN) and E(BN) are the total energy of WZ AlN and BN respectively. Figure 3 shows the alloy formation enthalpy ΔH. The positive sign of ΔH indicates that the ground state of these alloys at T = 0 corresponds to a tendency to phase separation into pure WZ constituents BN and AlN. Moreover, the magnitude of ΔH is relatively strong (i.e., for x = 0.5, ΔH = 170meV) suggesting that large miscibility gap can exist in this system.

The mechanical properties of BN-AlN alloys were further studied. The calculated elastic constants C_{ij} of wurtzite BN and AlN compounds and BAlN alloys are presented in Table II. The WZ phase of BN and AlN, which have a stable phase at room temperature, meet the mechanical stability criteria. Furthermore, the calculated elastic constants of BAl_3N_4, $BAlN_2$, and B_3AlN_4 compounds satisfy also the Born stability criteria.

The bulk modulus B_0 (calculated from the elastic constants), shear moduls (G), Young's modulus (E) and Poisson's ratio (ν) are given in Table III. Figure 4 manifests the change of E, B_0 and G with composition x. The composition dependence of B_0 is sublinear; whereas G, and more precisely E, shows significant superliner dependence on composition (i.e., strong deviation from VCA). Moreover, the Poisson's ratio ν is found rather relatively indifferent with respect to composition x. In order to evaluate the ductility of the material, the B_0/G values were calculated and are listed in Table III. Higher B_0/G values greater than 1.75

corresponds to a ductile material; while values less than 1.75 correspond to a brittle material. As shown in Table III, except AlN which indicate that this compound is a borderline material, for all other phases B_0/G values are less than 1.75, which reflects a brittle characteristic of those compounds.

The dynamical stability of cubic (BAl_3N_4, and B_3AlN_4) and tetragonal ($BAlN_2$) phases of BAlN alloys was tested from the calculation of the phonon dispersion curves along the high-symmetry lines (Figure 5). All frequencies are real, i.e., no imaginary phonon frequencies are found in the whole Brillouin zone for all phases, indicating the dynamical stability of BAl_3N_4, $BAlN_2$ and B_3AlN_4 ordered structures of BN-AlN systems.

Here we discuss the band gap dependence of $B_xAl_{1-x}N$ on B composition. It is well known that DFT underestimates severely the band gap by 50%-100%, that's why we used the LDA-1/2 method [28]. This approach competes well with more advanced method such as GW quasiparticle approach [29]. We obtain a direct band gap of 6.16eV ($\Gamma\rightarrow\Gamma$) for WZ AlN that is within the range of experimentally measured gaps (6.19eV [30], 6.23eV [22]). For WZ BN, we obtain a direct $\Gamma\rightarrow\Gamma$ (indirect, $\Gamma\rightarrow$K) band gap of 10eV (7.18eV). No experimental data are available so far. However, our calculated indirect band gap is close to GW calculations of 6.86eV [31] and scissor operator method of 6.8eV [5].

Figure 6 shows the resulting calculated change of direct band gap energy E_g ($\Gamma\rightarrow\Gamma$) for $B_xAl_{1-x}N$ alloys as function of composition x. The band gap bowing representing the deviation from a linear interpolation of the component band gaps of BN and AlN was calculated according to:

$$E_g(x) = (1-x)\, E_g(\text{AlN}) - x\, E_g(\text{BN}) - b\, x\, (1-x)$$

The values of $E_g(x)$ deviates from the linear behavior (i.e., the Vegard's law) and is characterized by the bowing parameter b. The band gap bowing parameter for the direct band gap is found giant (b = 11.62eV) for the entire range of composition. The calculated b is similar to other III-V-N mixed anion semiconductors (e.g., GaAsN, InAsN… [7, 22]). This is in contrast to common III-V semiconductors (e.g., GaAlAs), where it is relatively weak and composition-independent. Our results are consistent with the calculated bowing parameter of 8.55eV [6].

To understand the physical origins of b (i.e., having structural and electronic components), we determine the three physically distinct contributions of b [8]: volume deformation (VD), charge exchange (CE) and structural relaxation (SR). The VD term represents relative response of (AlN)BN to hydrostatic pressure from their equilibrium volume $V_{GaN}(V_{BN})$ to the

alloy $V(x)$. The CE term is related to a charge transfer in bringing AlN and BN at $V=V(x)$, and the SR term describes the change of the gap upon passing from the unrelaxed to the relaxed alloy, i.e., $V(x)\rightarrow V_{eq}$. The total optical band gap bowing is $b=b_{VD}+b_{CE}+b_{SR}$. At x = 0.5, we found b_{VD} = 4.88eV, b_{CE} = 3.64eV, and b_{SR} = -0.01eV yielding a total bowing parameter of 8.51eV. The volume deformation contribution b_{VD} is giant and can be correlated to the large mismatch of the lattice constants a of BN and AlN (~20%). The chemical electronegativity term b_{CE} is strong and scale with the strong electronegativity mismatch between B and Al atoms. Using Pauling"s electronegativities of 2.04 and 1.5 for B and Al atoms respectively, we have an electronegativity mismatch of 0.54 for B-Al. The bowing contribution due to the structural relaxation term b_{SR} is negligible. As found previously, b_{SR} gives weak contribution to mixed cation alloys [8]. According to our calculated total optical band gap bowing parameter at x = 0.5 (b = 8.51eV) and b~11.6eV for the entire range of composition, we can expect that b depends strongly on composition x.

4 Conclusion

In summary, a systematic search for stable compounds in BN-AlN alloys has been carried out using *ab initio* evolutionary algorithm. We have uncovered three structures, cubic BAl_3N_4 (space group *P*-43m) and B_3AlN_4 (space group *P*-43m) and tetragonal $BAlN_2$ (space group *P*-4m2). All those phases are thermodynamically unstable but mechanically and dynamically stable. State-of-the-art LDA-1/2 approach was used to determine the direct band gap of $B_xAl_{1-x}N$ alloys. We found an extreme optical band gap bowing parameter of b~11.6eV over the entire range of composition. Furthermore b is found composition-dependent. Our analysis evidences that b parameter for $x = 0.5$ mainly arises from structural and chemical effects.

References

[1] S. Watanabe, T. Takano, K. Jinen, J. Yamamoto and H. Ka-wanishi, Phys. Status Solidi C7 (2003) 2691.

[2] A. Nakajima, Y. Furukawa, H. Yokoya, and H. Yonezu, J. Cryst. Growth 278 (2005) 437.

[3] T. L. Williamson, N. R. Weiss-Bernstein, and M. A. Hoffbauer, Phys. Status Solidi 11 (2014) 462.

[4] X. Li, S. Sundarem, Y. El Gmili, F. Genty, S. Bouchoule, G. Patriache, P. Disseix, F. Réveret, J. Leymarie, J. P. Salvestrini, R. D. Dupuis, P. L. Voss, and A. Ougazzaden, J. Cryst. Growth 414 (2015) 119.

[5] M. Zhang and X. Li, Phys. Status Solidi B 254 (2017) 1600794.

[6] J.-X. Shen, D. Wickramaratne, and C. G. Van de Walle, Phys. Rev. Mater. 1 (2017) 065001.

[7] M. Ferhat, phys. stat. sol. (b) 241 (2004) R38.

[8] M. Ferhat and F. Bechstedt, Phys. Rev. B 65 (2002) 075213.

[9] A. Belabbes, M. Ferhat and A. Zaoui, Appl. Phys. Lett. 88 (2006) 152109.

[10] H. Benaissa, A. Zaoui, and M. Ferhat, J. Appl. Phys. 102 (2007) 113712.

[11] A. Belabbes, A. Zaoui and M. Ferhat, J. Phys.: Condens. Matter 19 (2007) 456212.

[12] A. Berghout, A. Zaoui, J. Hugel and M. Ferhat, Phys. Rev. B 75(2007) 205112.

[13] A. Belabbes, A. Zaoui, S. Laref and M. Ferhat, Solid State Commun 152 (2012) 1700.

[14] A. Jain, S. P. Ong, G. Hautier, W. Chen, W. D. Richards, S. Dacek, S. Cholia, D. Gunter, D. Skinner, G. Ceder, and K. A. Persson, Apl. Mater. 1 (2013) 011002 (2013), https://www.materialsproject.org

[15] G. Hautier, C. Fischer, V. Ehrlacher, A. Jain, and G. Ceder, Inorg. Chem. 50 (2011) 656.

[16] W. Kohn and L. J. Sham, Phys. Rev. 140 (1965) A1133.

[17] P. Giannozzi et al., J. Phys. : Condens. Matter 21 (2009) 395502.

[18] J. P. Perdew and A Zunger, Phys. Rev. B 23 (1981) 5048.

[19] A. Dal Corso, Phys. Rev. B 82 (2010) 075116.

[20] H. J. Monkhorst and J. D. Pack, Phys. Rev. B 13 (1976) 5188.

[21] S. Baroni, S. de Gironcoli, A. Dal Corso, and P. Giannozzi, Rev Mod. Phys. 73 (2001) 515.

[22] I. Vurgaftman, J. R. Meyer and L. R. Ram-Mohan, J. Appl. Phys. 89 (2001) 5815, and references therein.

[23] T. Soma, S. Sawaoka, and S. Saito, Mater. Res. Bull. 9 (1974) 755.

[24] Semiconductors: Data Handbook, 3rd ed., edited by O. Madelung (Springer, Berlin, 2004).

[25] K. Kim, W. R. L. Lambrecht, and B. Segall, Phys. Rev. B 53 (1996) 16310.

[26] M. Ueno, A. Onodera, O. Shimomura, and K. Tokemura, Phys. Rev. B 45 (1992) 10123.

[27] V. A. Pesin, Sverktverd. Matter. 6 (1980) 5.

[28] L. G. Ferreira, M. Marques, and L. K. Teles, Phys. Rev. B 78 (2008) 125116.

[29] M. S. Hybertsen and S. G. Louie, Phys. Rev. B 37 (1988) 2733.

[30] D. Brunner, H. Angerer, E. Bustarret, F. Freudenberg, R. Höpler, R. Dimitrov, O. Ambacher, and M. Stutzmann, J. Appl. Phys. 82 (1997) 5090.

[31] S. P. Gao, Comput. Mater. Sci. 61 (1992) 266.

[32] S. Azzi, A. Zaoui and M. Ferhat Solid State Commun 144 (2007) 245.

Table Captions

Table I: Calculated equilibrium structural parameters, for AlN, BAl_3N_4, $BAlN_2$, B_3AlN_4 and BN.

Table II: Calculated elastic constants (in GPa) of AlN, BAl_3N_4, $BAlN_2$, B_3AlN_4 and BN.

Table III: Calculated bulk modulus B_0 (in GPa), Young's modulus E (GPa), shear modulus G (in GPa), Poisson's ratio ν (GPa) and B_0/G.

Figure Captions

Figure 1: Crystal structures of $B_xAl_{1-x}N$ alloys: a) WZ-AlN, b) BAl_3N_4, c) $BAlN_2$, d) B_3AlN_4 and e) WZ-BN.

Figure 2: Calculated lattice constant a, lattice ratio c/a of $B_xAl_{1-x}N$ alloys as function of B composition.

Figure 3: Calculated formation enthalpy of $B_xAl_{1-x}N$ alloys.

Figure 4: Calculated bulk modulus B_0 (GPa), Young's modulus E (GPa), and shear modulus G (GPa) as function on B composition.

Figure 5: Phonon band structure and phonon density of states (PDOS) of a) BAl_3N_4, b) $BAlN_2$, and c) B_3AlN_4.

Figure 6: Band gap dependence of $B_xAl_{1-x}N$ on B composition.

Table I

Phase	*a*(Å)	*c/a*	*Space group*
AlN	3.088 3.112[a]	1.600 1.601[a]	$P6_3mc$
BAl_3N_4	4.162		*P*-43m
$BAlN_2$	2.774	1.475	*P*-4m2
B_3AlN_4	3.791		*P*-43m
BN	2.525 2.553[b]	1.653 1.656[b]	$P6_3mc$

[a]Ref.[22].

[b]Ref.[23].

Table II

	C_{11}	C_{12}	C_{13}	C_{33}	C_{44}	C_{66}
AlN	399	146	114	367	115	126.5
Expt.[a]	411	149	99	389	125	131
BAl_3N_4	371	183			212	
$BAlN_2$	596	41	182	593	223	103
B_3AlN_4	586	204			313	
BN	986	146	65	1097	345	420
Calc.[b]	987	143	70	1020	369	422

[a]Ref.[24].

[b]Ref.[25].

Table III

	B_0	E	G	ν	B_0/G
AlN	212(208[a])	311	124	0.25	1.71
BAl_3N_4	246	380	153	0.24	1.61
$BAlN_2$	282	460	187	0.23	1.51
B_3AlN_4	332	612	257	0.19	1.29
BN	402(410[b])	908	404	0.12	0.99

[a]Ref.[26].

[b]Ref.[27].

Figure 1

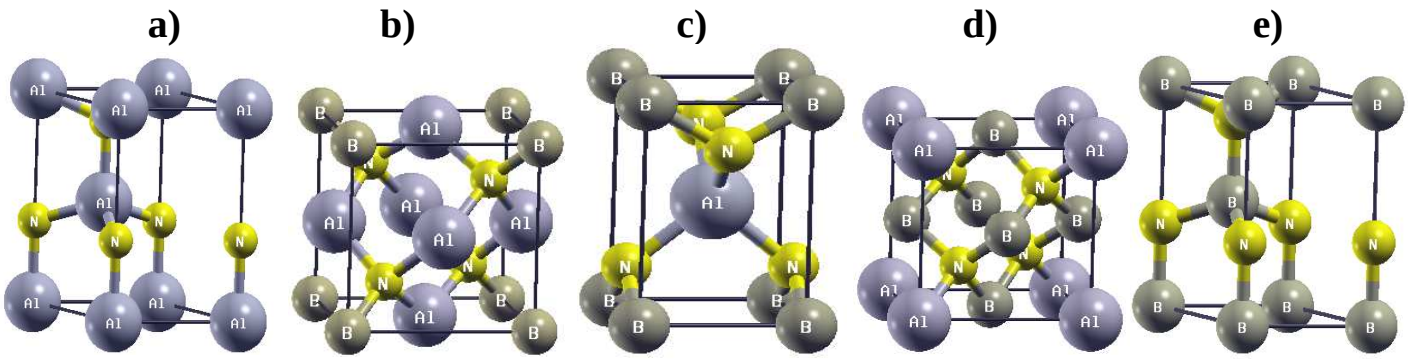

Figure 2

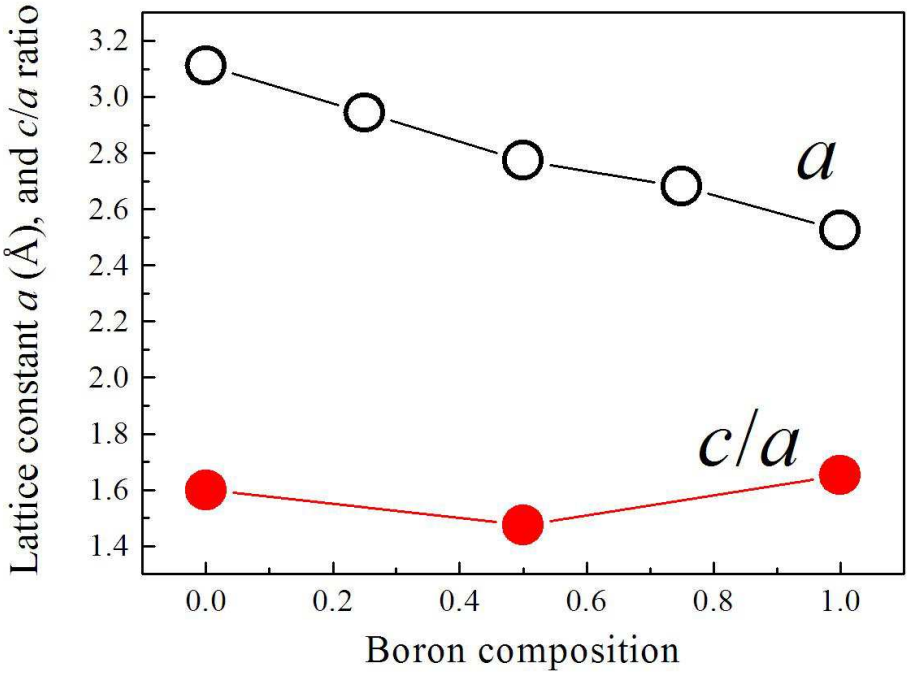

Figure 3

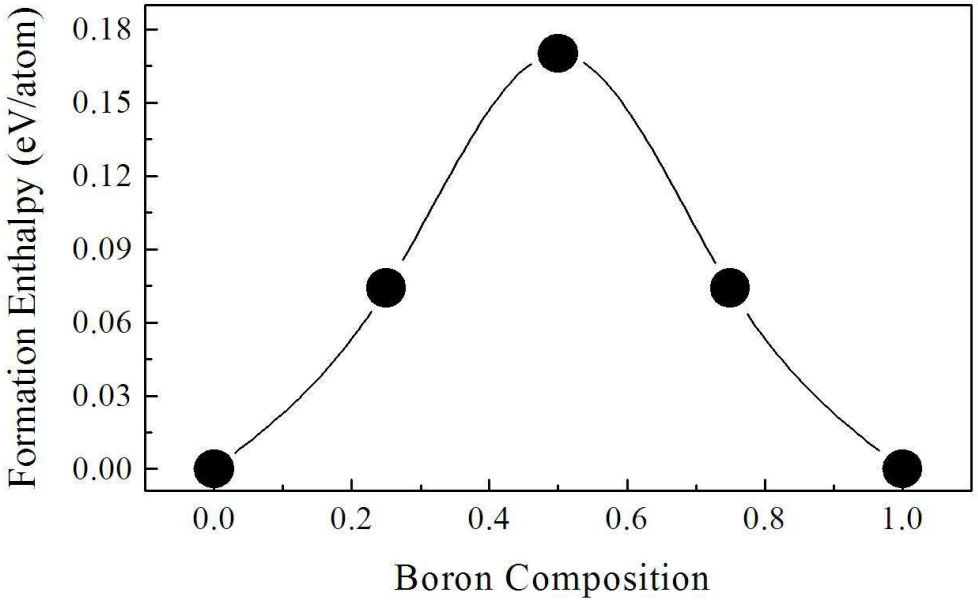

Figure 4

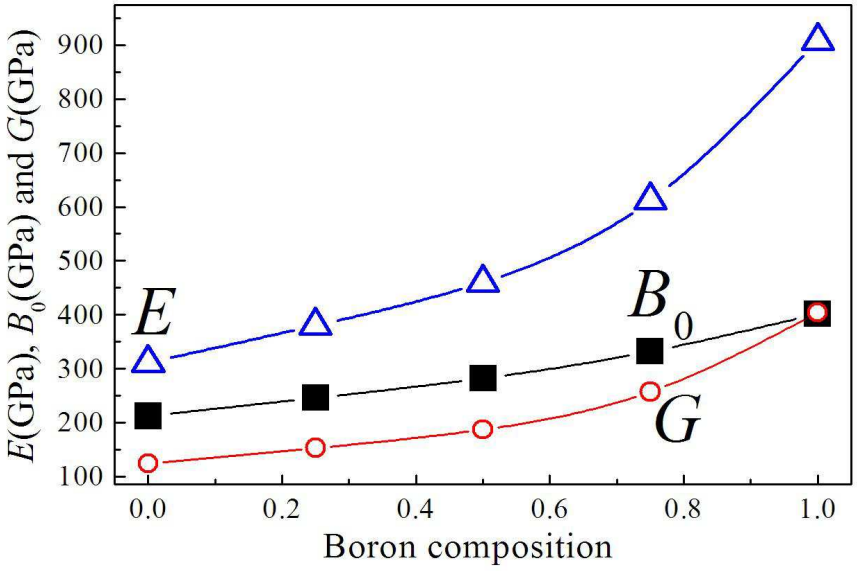

Figure 5

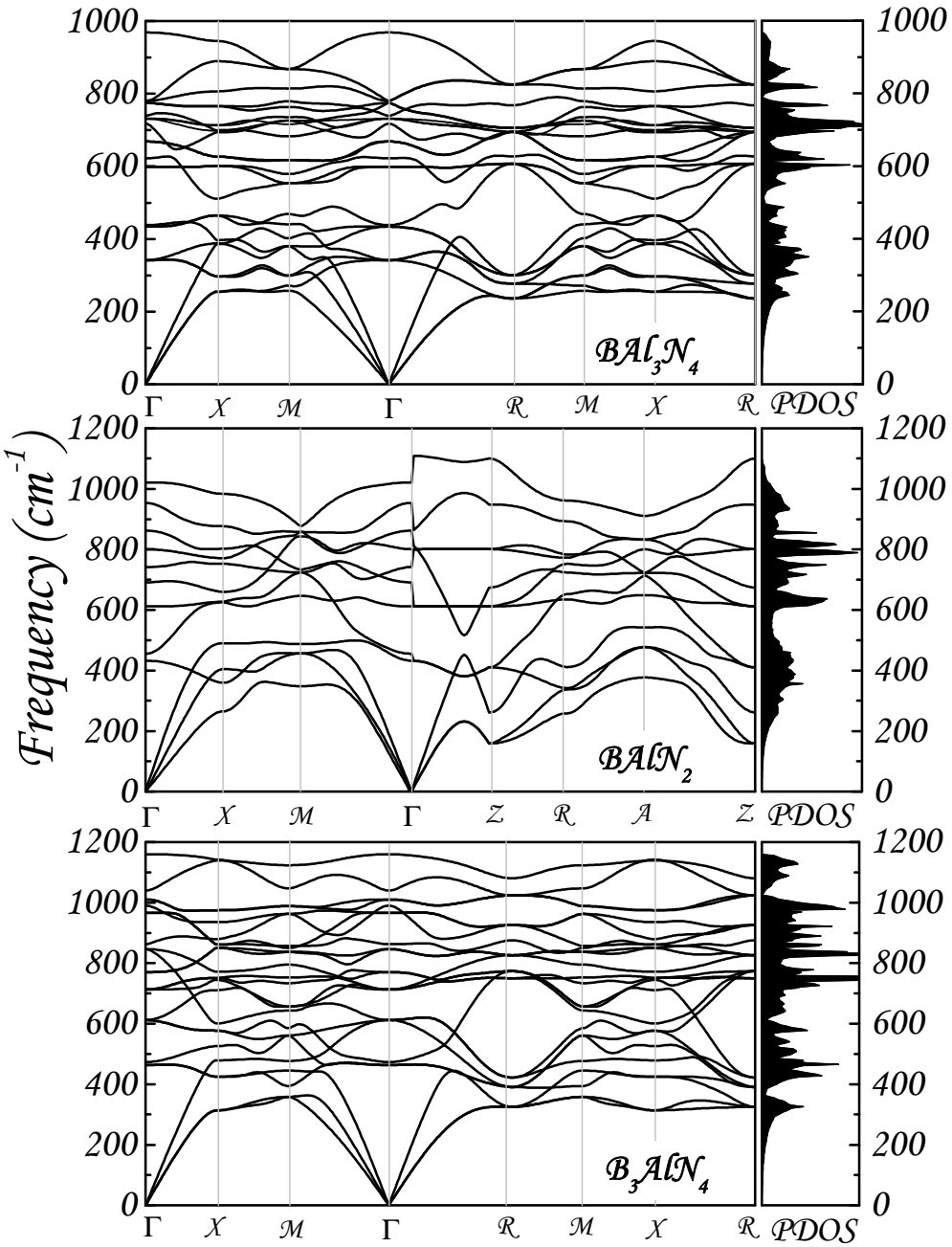
Frequency (cm-1)
BAl3N4
BAlN2
B3AlN4
PDOS
Γ X M Γ R M X R
Γ X M Γ Z R A Z
0 200 400 600 800 1000 1200

Figure 6

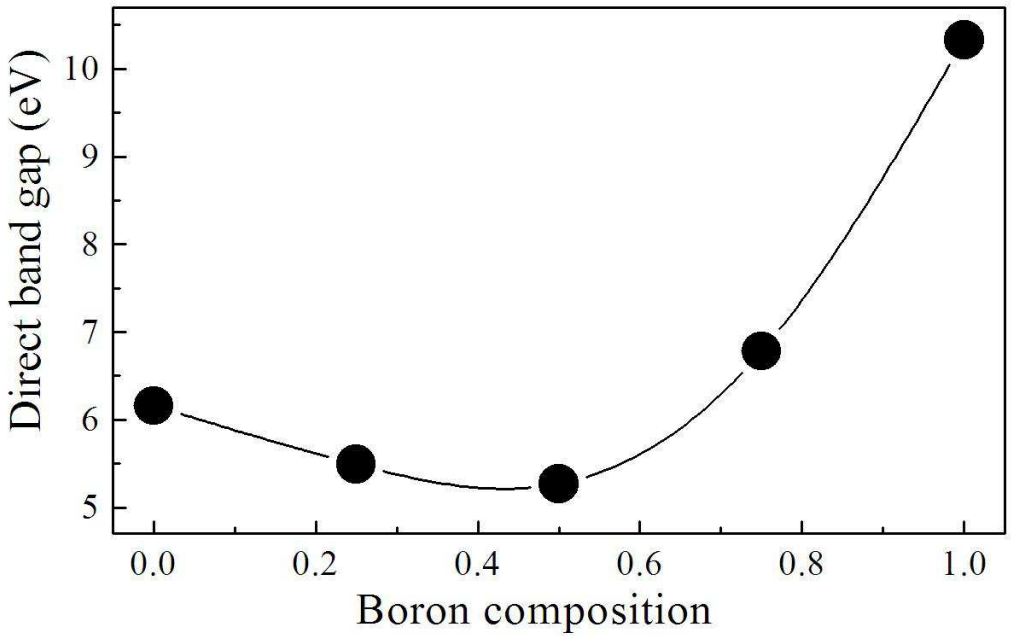
Direct band gap (eV)
10
9
8
7
6
5
0.0
0.2
0.4
0.6
0.8
1.0
Boron composition